minerals

MDPI

Article

Phlogopite $^{40}Ar/^{39}Ar$ Geochronology for Guodian Skarn Fe Deposit in Qihe–Yucheng District, Luxi Block, North China Craton: A Link between Craton Destruction and Fe Mineralization

Qiwei Feng [1,2], Mingbo Gao [2,3,*], Chao Fu [4,5], Siyuan Li [4,5,*], Yadong Li [1,2], Jilei Gao [1,2], Ming Ma [1,2], Zhaozhong Wang [1], Yidan Zhu [6], Binglu Wu [1,2], Zhuang Duan [2,7] and Zhicai Dang [4,5]

1 No. 1 Institute of Geology and Mineral Resources of Shandong Province, Jinan 250100, China; fqw0000002022@163.com (Q.F.); lydludi@sina.com (Y.L.); gjljn@163.com (J.G.); sddkmaming@163.com (M.M.); wangzhaozhong163@163.com (Z.W.); 13505408585@139.com (B.W.)
2 Shandong Engineering Research Center of High-Grade Iron Deposits Exploration and Exploitation, Jinan 250100, China; zduan_geology@163.com
3 Shandong Provincial Bureau of Geology & Mineral Resources, Jinan 250000, China
4 Tianjin Center of China Geological Survey, Tianjin 300170, China; fuchaocugb@163.com (C.F.); dangzhicai@163.com (Z.D.)
5 North China Center for Geoscience Innovation, China Geological Survey, Tianjin 300170, China
6 School of Resources and Environmental Engineering, Shandong University of Technology, Zibo 255049, China; 13854808103@163.com
7 Institute of Geophysical and Geochemical Exploration, Chinese Academy of Geological Sciences, Langfang 065000, China
* Correspondence: jngmb@126.com (M.G.); cgs-siyuanli@foxmail.com (S.L.)

Abstract: The Guodian Fe deposit is representative of the newly discovered Qihe–Yucheng high-grade Fe skarn ore cluster, Luxi Block, eastern North China Craton (NCC). The age of the Pandian Fe deposit remains elusive, which hinders the understanding of its metallogenic tectonic background. Phlogopites are recognized in syn-ore stages, and they are closely associated with magnetite in the Guodian skarn Fe deposit. Here, we carried out $^{40}Ar/^{39}Ar$ dating of phlogopite, which can place a tight constraint on the timing of Guodian iron mineralization and shed light on the geodynamic framework under which the Guodian Fe deposit formed. Ore-related phlogopite $^{40}Ar/^{39}Ar$ dating yielded $^{40}Ar/^{39}Ar$ plateau ages of 131.6 ± 1.7 Ma at 890–1400 °C, with the corresponding isochron age being 131.1 ± 2.6 Ma. These two ages are consistent within the error, indicating that they can represent the formation age of the Guodian iron deposit. The mineralization age overlaps the zircon U-Pb age of 124.4 Ma for ore-related Pandian pluton. This age consistency confirms that the iron skarn mineralization is temporally and likely genetically related to Pandian diorite. The present results, coupled with existing isotopic age data, indicate the Guodian skarn Fe deposit formed contemporaneously with large-scale skarn iron mineralization over the Luxi Block in the Late Mesozoic. The available data demonstrated that the eastern NCC was "destructed" in the Late Mesozoic, as marked by voluminous igneous rocks, faulted-basin formation, high crustal heat flow, and widespread metamorphic core complexes in the eastern part of the NCC. It is thus suggested that the Guodian Fe skarn deposits, together with other deposits of similar ages in the Luxi Block and even in the eastern NCC, were products of this craton destruction. Lithospheric extension and extensive magmatism related to the craton destruction may have provided sufficient heat energy, fluid, chlorine, and Fe for the formation of the Fe deposit.

Keywords: phlogopite; $^{40}Ar/^{39}Ar$ geochronology; Guodian Fe skarn deposit; Qihe–Yucheng Fe ore cluster; Luxi Block

check for updates

Citation: Feng, Q.; Gao, M.; Fu, C.; Li, S.; Li, Y.; Gao, J.; Ma, M.; Wang, Z.; Zhu, Y.; Wu, B.; et al. Phlogopite $^{40}Ar/^{39}Ar$ Geochronology for Guodian Skarn Fe Deposit in Qihe–Yucheng District, Luxi Block, North China Craton: A Link between Craton Destruction and Fe Mineralization. *Minerals* **2024**, *14*, 690. https://doi.org/10.3390/min14070690

Academic Editor: Urs Klötzli

Received: 13 April 2024
Revised: 19 June 2024
Accepted: 28 June 2024
Published: 1 July 2024

Copyright: © 2024 by the authors. Licensee MDPI, Basel, Switzerland. This article is an open access article distributed under the terms and conditions of the Creative Commons Attribution (CC BY) license (https://creativecommons.org/licenses/by/4.0/).

1. Introduction

There is a serious paucity of high-grade iron ore (TFe grade ≥ 50%) in China, of which the average iron ore grade is only approximately 30% [1]. The skarn Fe deposit

is one of the main categories of Fe and accounts for the most important type of high-grade Fe ore in China [2]. Precise dating of skarn Fe deposits is of critical importance in establishing the temporal relation to the geodynamic framework under which they formed and in developing a comprehensive genetic model. Numerous attempts have been made to constrain the timing of skarn Fe deposits, mainly by U-Pb dating of U-bearing hydrothermal accessory minerals, such as zircon [3], titanite [4], $^{40}Ar/^{39}Ar$ dating of K-bearing alteration phases, such as phlogopite [5,6], and U-Pb dating of zircon from ore-related intrusions [7,8].

The North China Craton (NCC) hosts numerous skarn Fe deposits (Figure 1), accounting for one of the largest high-grade iron ore provinces in China. Iron skarn deposits of the NCC cluster in several major districts, forming two roughly NNE-striking belts in the central–eastern NCC (Figure 1) [4]. The eastern belt consists of the Luxi and Xu-Huai districts, and the western belt comprises the Southern Taihang, Linfen, and Taiyuan ore fields. Previous studies have shown that the NCC experienced a large-scale reactivation, peaking in the early Cretaceous [9–18], as manifested by voluminous magmatism, faulted-basin formation, high crustal heat flow, and widespread metamorphic core complexes in the eastern part of the craton. Researchers named this reactivation craton destruction. Previous geochronological studies indicate that the skarn Fe deposits and associated productive magmas in the eastern NCC that catastrophically formed in the Early Cretaceous [4,19,20] coincide temporally with the peak of craton destruction in the eastern NCC, implying they are the response and products of the lithospheric thinning and destruction of the NCC [21,22].

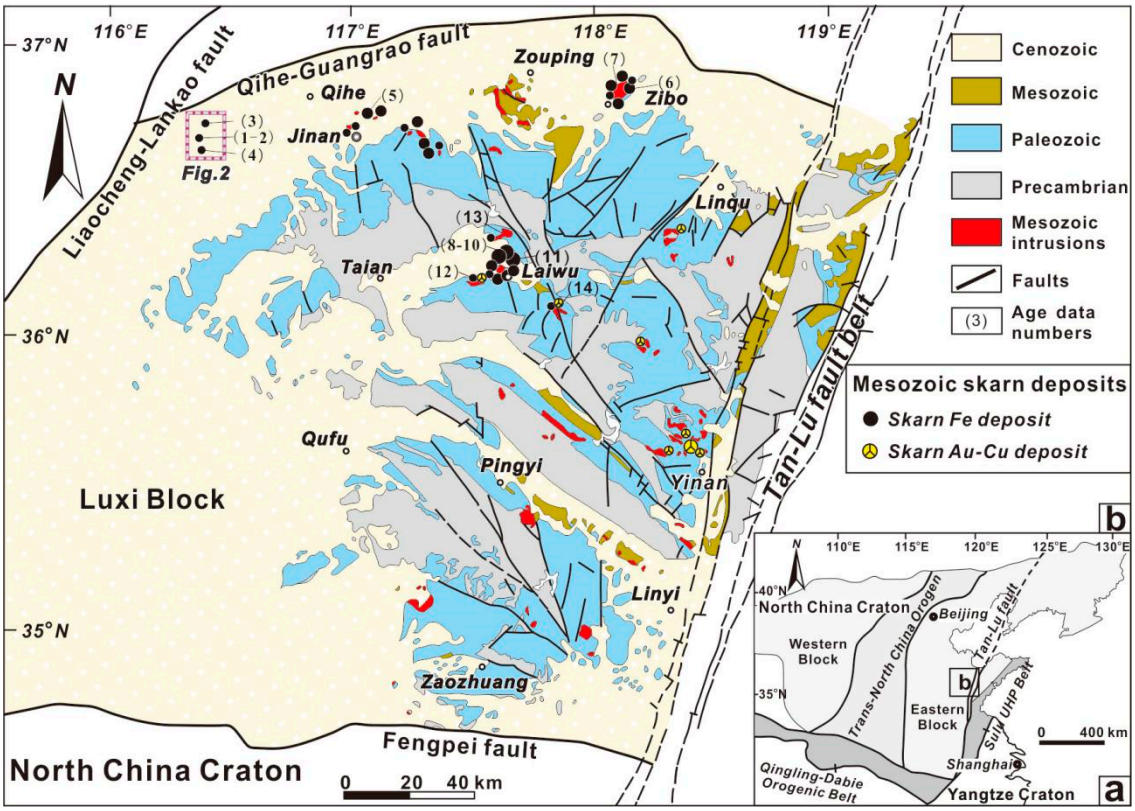


Figure 1. Simplified geological map of the North China Craton showing the major tectonic divisions and the location of the Luxi Block (**a**) and a geological map of the Luxi Block showing the distribution of major Mesozoic intrusions and skarn deposits (**b**); The numbers (1–14) correspond to the numbers of skarn Fe deposits in Table 3 (revised from [5]).

The Guodian iron deposit, located in the Qihe-Yucheng district, Luxi Block, eastern NCC, is a high-grade iron skarn deposit discovered recently in the deep-buried area of the northwestern part of the Luxi Block. The magnetite ore bodies of the Guodian deposit

are deeply buried and partly hosted in the Carboniferous and Permian strata, different from the other skarn Fe deposits in the Luxi Block, whose ore bodies are found in the near-surface zone and solely hosted in the Ordovician strata. The Guodian deposit has attracted much research attention because of its distinctiveness. However, current research studies are focused predominantly on metallogenic prediction and exploration techniques and methods [23–25], whereas little attention has been paid to diagenetic and metallogenic chronology. Only the ages of ore-related Litun, Dazhang, and Pandian intrusive rocks have been determined using the zircon U-Pb dating method until now [8,26]. The timing of the Guodian Fe deposit has not yet been tightly constrained, which hampers our understanding of the relationships between Fe mineralization and associated intrusive rocks, which in turn hinders us from exploring the probable links between the formation of the Guodian Fe deposit and destruction of the NCC.

In this paper, we integrated field, textual, and geochemical data of phlogopite to document their hydrothermal origin. We then conducted $^{40}Ar/^{39}Ar$ isotope analysis of phlogopite grains coexistent with magnetite to determine the metallogenic age of the Guodian iron deposit accurately. The results allow us to better understand ore genesis and constrain metallogenic geological background. The present study yields new insight into the metallogenesis of high-grade iron deposits in the Qihe-Yucheng region, which, in turn, have implications for iron ore prospecting.

2. Geological Background

The Tanlu Fault Zone divides Shandong Province into the Luxi Block and Jiaodong peninsula. The Luxi Block is located in the southeast of the North China Craton, west of the Tanlu Fault Zone, east of the Liaocheng–Lankao Fault Zone, south of the Qihe–Guangrao Fault Zone, north of the Fengpei Fault Zone, and adjacent to the Dabie–Sulu ultra-high pressure collision zone in the southeast. The rock outcrops in the Luxi Block mainly include the Mesoarchean Erathem granulite of the Yishui group, Neoarchean amphibolite, gneiss, leptynite and TTG rock series of the Taishan group, Paleoproterozoic metasediments, metavolcanic rocks and granitoids, Neoproterozoic sedimentary rocks, Paleozoic carbonatites interbedded with clasolites, Mesozoic terrestrial clastic rocks interbedded with sedimentary volcanic rocks, and Cenozoic sediments [27]. The interior of the Luxi Block is characterized by alternating depressions and uplifts, reflecting a typical basin–mountain structure, along with the development of radiating fractures and concentric ring fractures [5]. Magmatisms are frequent in the block and are characterized by regional zonation, multi-cyclicity, and polygenetic types. Most of them are early Precambrian magmatite, accounting for approximately 90% of the total area of magmatic rock outcrops in the block. The rock bodies related to mineralization are primarily Mesozoic magmatic rocks, whose activities are relatively strong, including the magmatization of both the Middle Jurassic and Early Cretaceous periods (Figure 1).

In the Qihe–Yucheng ore district, northwestern part of the Luxi Block (Figure 1b), a series of major breakthroughs have been made in high-grade iron ore prospecting over the years, including three skarn-type high-grade iron deposits that have been successively discovered in Litun, Dazhang, and Guodian (Figure 2), positioning it as an important high-grade iron ore-mineral-concentrated area in the Luxi Block. The strata of the Qihe–Yucheng ore district are the Neoarchean Taishan rock group, Paleozoic Cambrian, Ordovician, Carboniferous, Permian, and Cenozoic Neogene rock groups, and quaternary rock groups widely distributed on the surface. Among them, the Ordovician Majiagou group carbonates are widespread and important skarn-type iron ore-controlling wall rocks in the area. Its tectonic activities are intense, with faults occupying first place and folds coming second. Faults are generally spread in the NNE and NW directions, forming the boundary of subsurface bulging and subsidence. Igneous rocks are widely distributed in the area as mostly Mesozoic intrusions (intermediate–basic rocks).

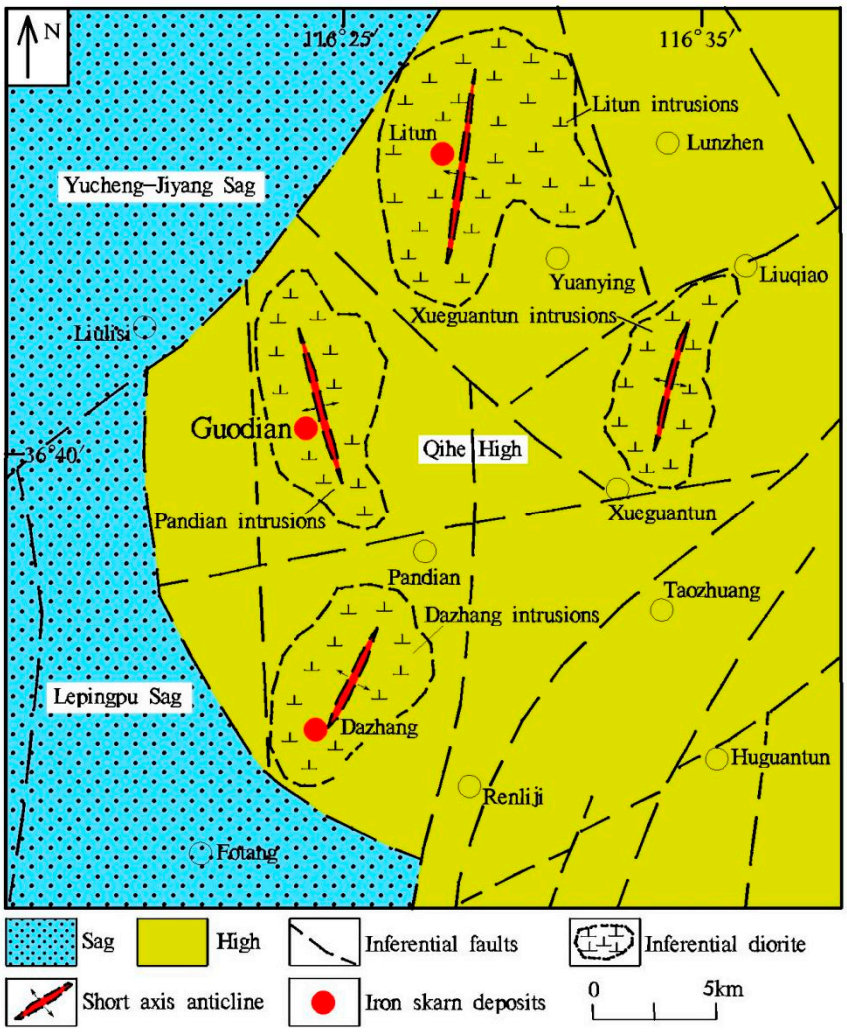


Figure 2. Geological structure diagram of the Qihe–Yucheng area (revised from [23]).

3. Ore Deposit Geology

Lying in the central Qihe–Yucheng ore district, the Guodian iron mine belongs to a Quaternary cover area. According to available borehole log data and the interpretation of geophysical results, its deep formations consist of the Ordovician Majiagou group, the Carboniferous–Permian Yuemengou group, the Permian Shihezi group, and Neogene. The Ordovician Majiagou group is closely related to mineralization, followed by the Carboniferous and Permian groups. The ore bodies are mainly hosted in the contact zone between intrusive rocks and Ordovician carbonate, which are larger in scale than the ore bodies hosted in the Carboniferous–Permian formation (Figure 3). The mine is of a faulted structure, principally the Wutou Fault and the Juzhen Fault, and the nature and occurrence of the faults are mainly controlled by regional faulting tectonics such as the Qiguang Fault, the Liuji Fault, and the Dong'e Fault. The magmatic rocks within the area are concealed Pandian intrusion, consisting mostly of hornblende pyroxene diorite, diorite, and quartz diorite. These rocks have been altered to varying degrees and interspersed with a bit of fine-grained rock, monzonite, and diabase. Diorite intruded mainly into the Ordovician strata and generated iron mineralization in the contact zone between intrusive rocks and Ordovician carbonates, which is an important prospecting site in the area [23,28].

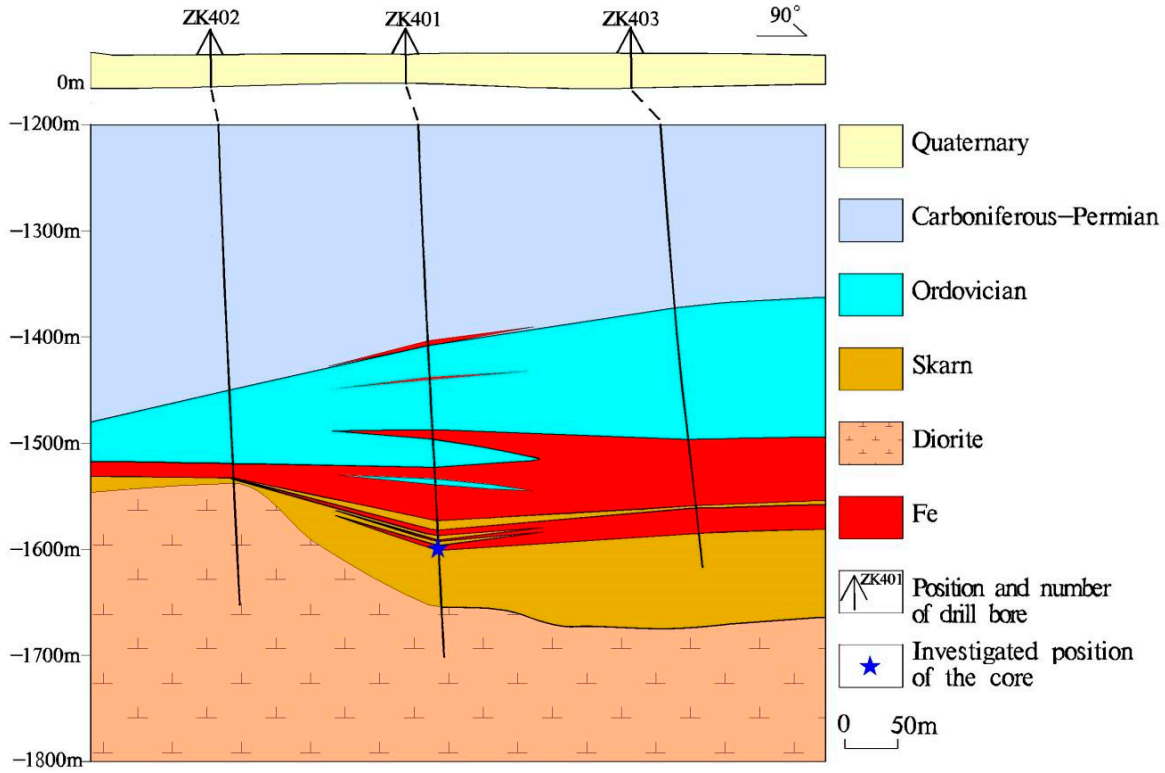


Figure 3. Geological profile of the no. 4 exploration line in the Guodian mining area.

At the present stage, a total of eight magnetite ore bodies, mostly in stratoid forms, have been delineated in the Guodian iron mine. The dip of the currently controlled ore body is NE, with an inclination in the range of 5 to −14°, and the ore-bearing elevation is in the range of −1037 to −1602 m. The highest total Fe grade of a single ore body sample is 67.44%, and the average grade of the main ore bodies is 57.19%. The ore bodies mainly occur in and near the contact zone between Pandian diorite and Ordovician limestone, dolomite, and some veins at the interlayer slip position of the Carboniferous–Permian clastic rock stratum (Figure 3). Most of the ore textures are euhedral–granular to hypidiomorphic granular, and others are metasomatic, interstitial, and poikilitic textures; the ore structures are mainly compact and massive structures (Figure 4a,c), plus a few banded (Figure 4b), disseminated and vein structures (Figure 4e). The ore minerals are primarily magnetite, followed by pyrite, pyrrhotite, chalcopyrite, sphalerite, etc.; nonmetallic minerals mainly include tremolite, diopside, olivine, serpentine (Figure 4d), and epidote, as well as a small amount of phlogopite, calcite (Figure 4f), chlorite, feldspar, and quartz.

Alteration happens to varying degrees inside the surrounding rocks at both sides of the ore bodies as the rock mass develops, resulting in skarnization, potassium feldspar, serpentinization, sericitization, epidotization, and chloritization. Skarnization is distributed in the contact zone between intrusive rocks and carbonate rocks. Potassic alteration is the most common alteration in diorite, and the sericitization, epidotization, and chloritization of rock mass are often superimposed on potassic feldspar. Among the rock, plagioclase is mostly metasomatized by potassic feldspar, giving the rock a color resembling the redness of flesh. Epidotization is widely developed in the surrounding rock at both sides of the ore bodies, skarn, and rock mass, and the epidotization in the rock mass often overlaps with sericitization and coexists with chlorite. Sericitization is relatively developed in the rock mass, strongly altered, and always superimposed on early potassium feldspar. Plagioclase is commonly altered into sericite, making the protolith look greenish blue [23,28].

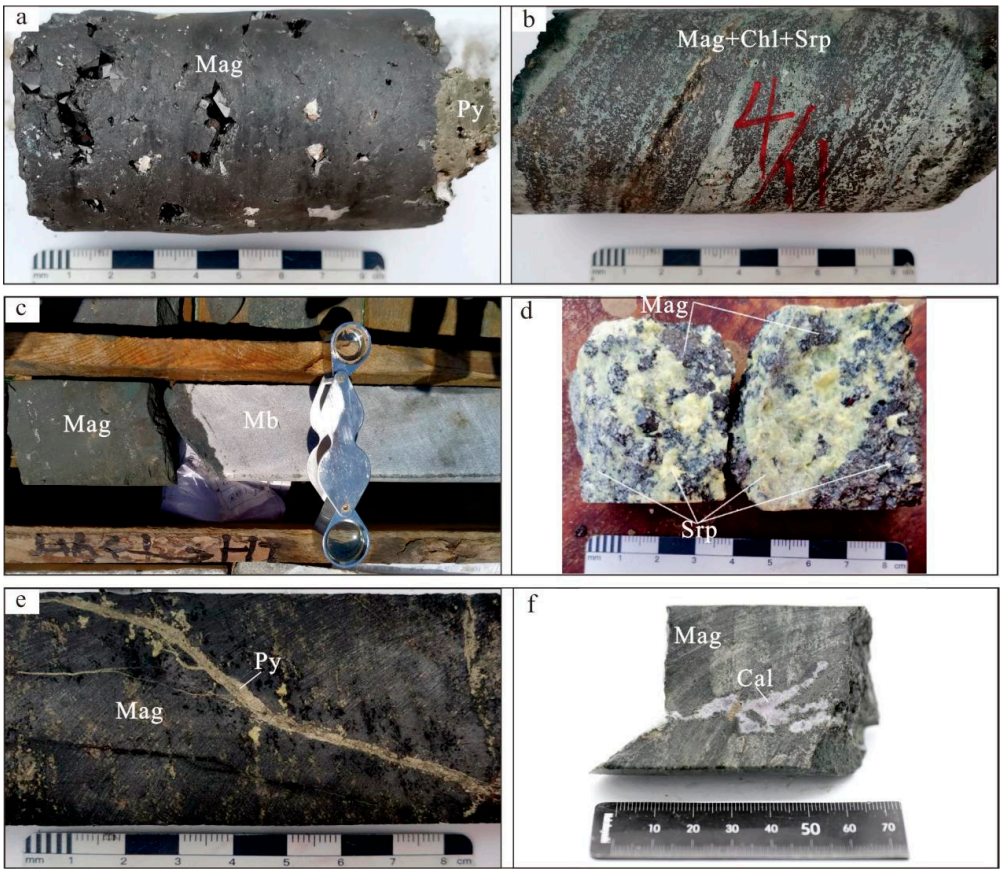


Figure 4. Photographs of typical iron ores from the Guodian iron deposit. (**a**) massive magnetite orebodly with pyrite; (**b**) banded magnetite orebodly with chlorite and serpentine; (**c**) magnetite orebodly in direct contact with marble; (**d**) magnetite orebodly was overprinted by serpentine; (**e**) disseminated magnetite was intruded by laterpyrite veins; (**f**) disseminated magnetite was intruded by calcite veins. Mag—magnetite; Chl—chlorite; Srp—serpentine; Mb—marble; Py—pyrite; Cal—calcite.

The hydrothermal metallogenic period of Guodian iron ore can be divided into prograde skarn stage, retrograde skarn stage, sulfide stage, and carbonate stage (Figure 5) according to vein interpenetration and the paragenetic association of minerals and surrounding rock alteration, among other characteristics. Diopside and small amounts of garnet, wollastonite, spinel, and olivine are developed mostly during the prograde skarn stage. Diopside skarn and garnet skarn are relatively developed in the Guodian iron deposit (Figure 6a). The retrograde skarn stage is the main stage for magnetite formation, which is characterized by the paragenesis of phlogopite, tremolite, serpentine, low levels of hydrous silicate minerals such as epidote and actinolite, and magnetite (Figure 6b,c). In the figures, it can be seen that magnetite is distributed in a subhedral–xenomorphic granular texture among phlogopite, tremolite, and other minerals, and serpentines are formed under metasomatism at the prograde skarn stage such as garnet and olivine (Figure 6b–d). Pyrite, chalcopyrite, pyrrhotite, quartz, and other minerals are primarily formed during the sulfide stage, and it can be observed under the microscope that pyrite, chalcopyrite, sphalerite, galena, and other sulfides are interwoven and replaced with early-formed magnetite ores (Figure 6e). Calcite at the carbonate stage is mainly veined into early sulfide and magnetite ores (Figure 6f).

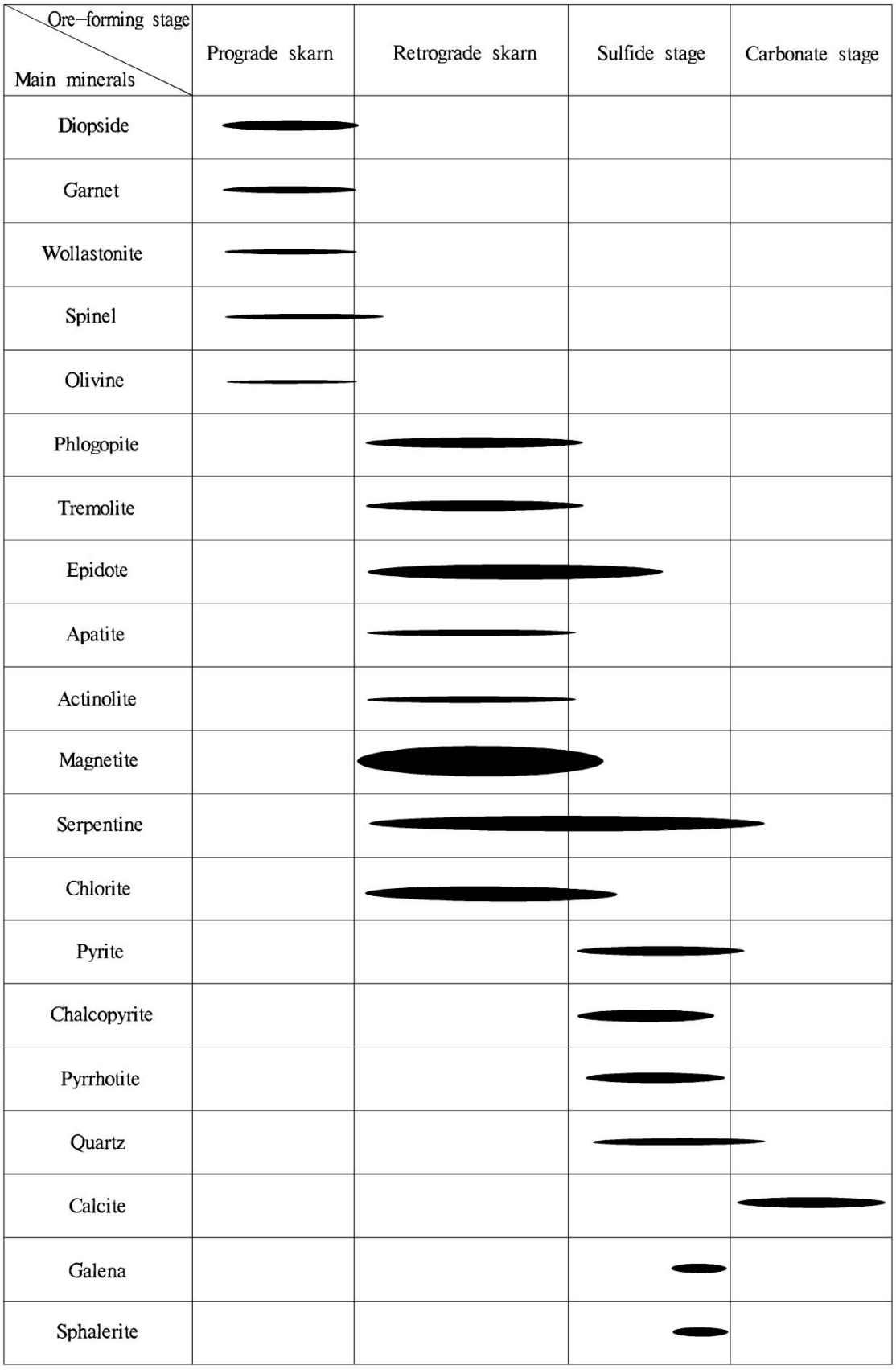


Figure 5. Paragenetic mineral table for the Guodian skarn iron deposit.

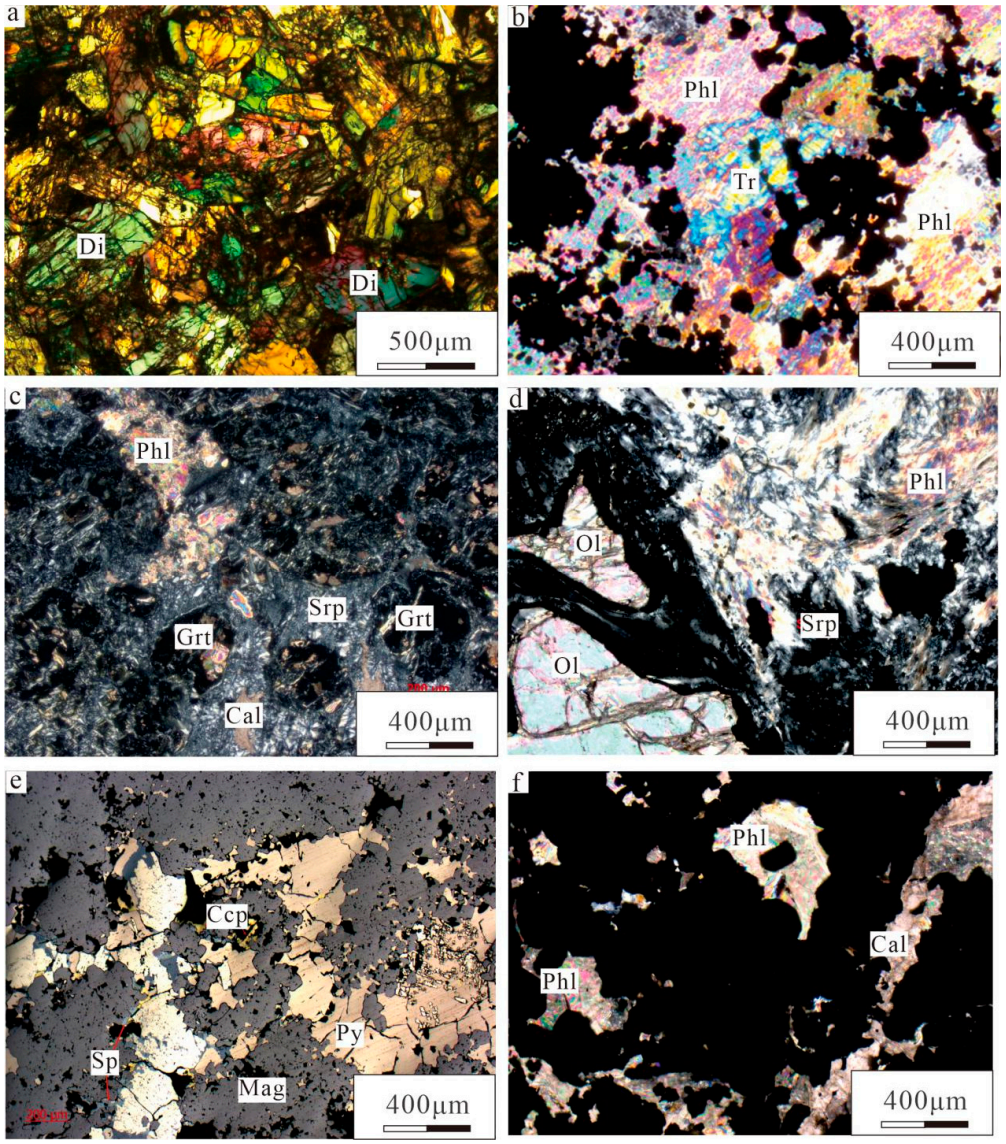


Figure 6. Micrographs of typical iron ores from the Guodian iron deposit. (**a**) diopside skarn is relatively developed; (**b**) magnetite is closely associated with phlogopite and tremolite; (**c**) magnetite is closely associated with phlogopite, garnet, serpentine, and tremolite; (**d**) magnetite is closely associated with phlogopite, serpentine and olivine; (**e**) the pyrite, chalcopyrite, sphalerite are interwoven and replaced with early-formed magnetite ores; (**f**) calcite veins intruded into into early sulfide and magnetite ores. Di—diopside; Ol—olivine; Grt—garnet; Phl—phlogopite; Srp—serpentine; Tr—tremolite; Mag—magnetite; Py—pyrite; Ccp—chalcopyrite; Cal—calcite; Sp-sphalerite.

4. Sampling and Analytical Methods

The test sample (GD-21) was collected from a magnetite ore body in the Guodian iron mine, which is a phlogopite-bearing massive magnetite. The sample is for the most part composed of skarn minerals such as magnetite, pyrite, phlogopite, and serpentine, whereas the phlogopite aggregates are closely associated with magnetites and a few pyrites in sparsely disseminated or porphyritic patterns (Figure 7). The monomineral can be seen by the naked eye as a complete flake crystal with a particle size of 0.1–0.8 cm. It is brown to dark brown and has a semi-metallic luster, with its cleavage surface radiating a pearly luster. The samples were crushed and sieved on 60–80 mesh, and phlogopite was selected under the binocular lens. The pure phlogopite (purity > 99%) was cleaned by ultrasound. Every cleaned sample and neutron fluence monitor was wrapped in aluminum foil, and then nine wrapped samples and four monitors as a group were arranged in one aluminum foil tube

with two monitors on the two ends and two between every three samples. The samples and monitors wrapped in aluminum foil were multicrystal aliquots. Then, several aluminum foil tubes were sealed into quartz bottles. The bottle was irradiated for 4320 min in a nuclear reactor. The monitor irradiated together with the samples is an internal standard named Fangshan biotite (ZBH-25) with a reference age of 132.7 ± 1.2 Ma, and its potassium content is 7.6%. Relevant tests were conducted in the Ar-Ar Laboratory, Institute of Geology, Chinese Academy of Geological Sciences.

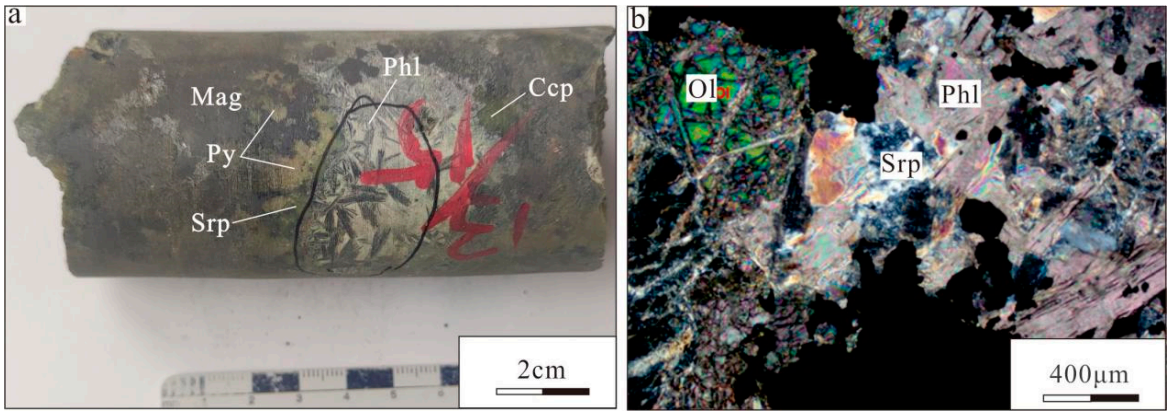


Figure 7. Representative hand specimens and micrographs of phlogopite-bearing iron ores from the Guodian iron deposit. (**a**) the sample is composed of skarn minerals such as magnetite, pyrite, phlogopite, and serpentine, whereas the phlogopite aggregates are closely associated with magnetites and a few pyrites in sparsely disseminated or porphyritic patterns; (**b**) phlogopite, serpentine and olivine are closely associated with magnetite. Mag—magnetite; Srp—serpentine; Phl—phlogopite; Py—pyrite; Ccp—chalcopyrite; Ol—olivine.

The samples were heated by a graphite furnace. The heating–extraction duration for each temperature increment was 10 min, and then the released gases were purified for 20 min. After the purification, the gases were analyzed by Mass Spectrometer GV Helix MC. The analysis for each temperature increment included 20 cycles, which needed to regress to time zero to obtain the measured isotopic ratios. Then, the measured isotopic ratios were corrected for mass discrimination, the atmospheric Ar component, blanks, and irradiation-induced mass interference. The correction factors of interfering isotopes produced during irradiation were determined by analysis of irradiated pure K_2SO_4 and CaF_4, and their values are $(^{36}Ar/^{37}Aro)_{Ca}$ = 0.0003863 ± 0.00002357, $(^{40}Ar/^{39}Ar)_K$ = 0.01276 ± 0.001289, $(^{39}Ar/^{37}Aro)_{Ca}$ = 0.003023 ± 0.00042. All ^{37}Ar were corrected for radiogenic decay. The decay constant of ^{40}K used was $\lambda = 5.54310^{-10}$ a^{-1} [29]. The atmospheric ratio of $^{40}Ar/^{36}Ar$ adopted was 295.5 [30]. The calculations of $^{40}Ar/^{39}Ar$ data were performed by the software ArArCALC [31]. For meaningful age plateaus, ArArCALC software used the following criteria. Incremental heating steps that have ages falling within the $1.96(\sigma_1{}^2+\sigma_2{}^2)1/2$ confidence envelope [32], where σ_1 and σ_2 are the standard deviations of the ages. In addition, the high-temperature plateaus that include more than three concordant incremental heating steps should represent >50% of the total amount of $^{39}Ar_k$ released [33–35]. The plateau age is the weighted mean age of the included steps, with the weighting factor being the inverse square of the age uncertainties. ArArCALC software allows the user to force plateaus to be calculated on certain steps, not choosing steps on their own according to the statistical method. The steps used to calculate the isochron ages were the same steps as the ones used to calculate the plateau age. The plateau age error and isochron age error are both 2σ.

5. Test Results

The $^{40}Ar/^{39}Ar$ isotopic dating results of mineralized and altered phlogopite in the Guodian iron mine are shown in Table 1, and the $^{40}Ar/^{39}Ar$ apparent age spectrum drawn

from the data is shown in Figure 8. The Ar-Ar experiment of phlogopite underwent a total of 14 heating stages. It can be seen in Table 1 that the apparent age of the sample is relatively young at the low-temperature exothermic stage, which might be caused by low-temperature crystal lattice defects of the mineral or a small amount of Ar loss on the mineral surface [36–38]. However, the temperature gradually increased from 650 °C to 1400 °C at the high-temperature exothermic stage, forming a basically undisturbed age spectrum (Figure 8). There was little difference among the apparent ages at the eight temperature stages of 890–1400 °C. The plateau age is 131.64 ± 1.69 Ma (MSWD = 36.99), corresponding to a ^{39}Ar precipitation of 91.35%. The ^{39}Ar/^{36}Ar-^{40}Ar/^{39}Ar isochron age is 131.10 ± 2.58 Ma (MSWD = 30.50, Figure 6), and the two ages are identical within the error range. In addition, the sample also showed a good inverse isochron age (130.11 ± 2.74 Ma, MSWD = 31.66; Figure 8), consistent with its plateau age.

Table 1. Sericite ^{40}Ar/^{39}Ar stepwise heating data (Sample GP-21) from the Guodian deposit.

Stage	Temperature (°C)	^{36}Ar [V]	^{37}Ar [V]	^{38}Ar [V]	^{39}Ar [V]	^{40}Ar [V]	40(r)/39(k)	±2σ	Age	±2σ (Ma)
1	650	0.0006111	0.0014474	0.0006399	0.0194853	0.20707	1.35719	±1.07573	5.67	±4.49
2	700	0.0008191	0.0018672	0.0014131	0.0479480	0.53465	6.09557	±0.51705	25.34	±2.13
3	740	0.0006790	0.0010850	0.0007522	0.0289415	0.93576	25.39494	±1.01684	103.31	±4.02
4	780	0.0012697	0.0038268	0.0019475	0.0698092	2.77303	34.34818	±0.47695	138.37	±1.85
5	820	0.0003878	0.0022915	0.0018773	0.0747677	2.74966	35.23811	±0.23765	141.82	±0.92
6	860	0.0005383	0.0048232	0.0042820	0.1746391	6.01760	33.54046	±0.18276	135.23	±0.71
7	890	0.0005312	0.0047771	0.0087042	0.3552671	11.82105	32.82266	±0.13381	132.44	±0.52
8	920	0.0007925	0.0039318	0.0208988	0.8652336	28.31166	32.43965	±0.10900	130.95	±0.42
9	950	0.0007064	0.0033577	0.0176964	0.7348026	24.14709	32.56683	±0.12146	131.45	±0.47
10	990	0.0011850	0.0051861	0.0137757	0.5563839	18.64310	32.86823	±0.14694	132.62	± 0.57
11	1030	0.0013723	0.0041595	0.0097853	0.3940666	13.57517	33.41007	±0.13906	134.73	± 0.54
12	1080	0.0019651	0.0084992	0.0119605	0.4784379	16.16810	32.57155	±0.12096	131.47	± 0.47
13	1200	0.0024833	0.0236282	0.0241768	0.9832604	32.25763	32.05353	±0.11515	129.45	± 0.45
14	1400	0.0002591	0.0039277	0.0006847	0.0238091	0.84498	32.29633	±1.94521	130.39	± 7.58

Stage	Temperature (°C)	Time (days)	^{40}Ar(r) (%)	^{39}Ar(k) (%)	K/Ca	±2σ	^{40}Ar/^{39}Ar	^{37}Ar/^{39}Ar	^{36}Ar/^{39}Ar	^{40}Ar(moles) (×10^{-11})
1	650	120.604	12.77	0.41	5.8	±4.2	10.6272	0.0743	0.0314	408.14
2	700	120.604	54.66	1.00	11.0	±5.3	11.1506	0.0389	0.0171	10.54
3	740	120.604	78.53	0.60	11.5	±6.2	32.3328	0.0375	0.0235	18.44
4	780	120.604	86.45	1.45	7.8	±2.4	39.7230	0.0548	0.0182	54.66
5	820	120.604	95.81	1.56	14.0	±3.4	36.7761	0.0306	0.0052	54.20
6	860	120.604	97.33	3.63	15.6	±2.5	34.4573	0.0276	0.0031	1.19
7	890	121.604	98.64	7.39	32.0	±6.8	33.2737	0.0134	0.0015	2.33
8	920	121.604	99.14	18.00	94.6	±23.9	32.7214	0.0045	0.0009	5.58
9	950	121.604	99.10	15.29	94.1	±50.0	32.8620	0.0046	0.0010	4.76
10	990	121.604	98.09	11.58	46.1	±16.1	33.5076	0.0093	0.0021	3.68
11	1030	121.604	96.98	8.20	40.7	±13.3	34.4489	0.0106	0.0035	2.68
12	1080	121.604	96.38	9.95	24.2	±4.5	33.7935	0.0178	0.0041	3.19
13	1200	121.604	97.70	20.45	17.9	±1.9	32.8068	0.0240	0.0025	6.36
14	1400	121.604	90.96	0.50	2.6	±1.3	35.4896	0.1650	0.0109	1.67

Note: Exposure parameters of phlogopite J = 0.00232080 ± 0.00001160. The sample weight of phlogopite is 14.95 mg. Decay constant ^{40}K = 5.543 ± 0.049 E−10 1/a. Decay constant ^{39}Ar = 2.940 ± 0.016E−07 1/h. Decay constant ^{37}Ar = 8.230 ± 0.012 E−04 1/h. Decay constant ^{36}Cl = 2.257 ± 0.015 E−06 1/a. Decay constant ^{40}K(EC,β^{+}) = 0.580 ± 0.009 E−10 1/a. Decay constant ^{40}K(β^{-}) = 4.950 ± 0.043 E−10 1/a. Atmospheric ratio 40/36(a) = 295.50. Atmospheric ratio 38/36(a) = 0.1869. Production ratio 39/37(ca) = 0.003023 ± 0.000420. Production ratio 36/37(ca) = 0.000386 ± 0.000024. Production ratio 40/39(k) = 0.012760 ± 0.001289. Production ratio 38/39(k) = 0.012110. Production ratio 36/38(cl) = 262.80 ± 1.71. Scaling ratio K/Ca = 0.430. Abundance ratio ^{40}K/K = 1.1700 ± 0.0100 E−04. The bold data were used to calculate the age of the plateau.

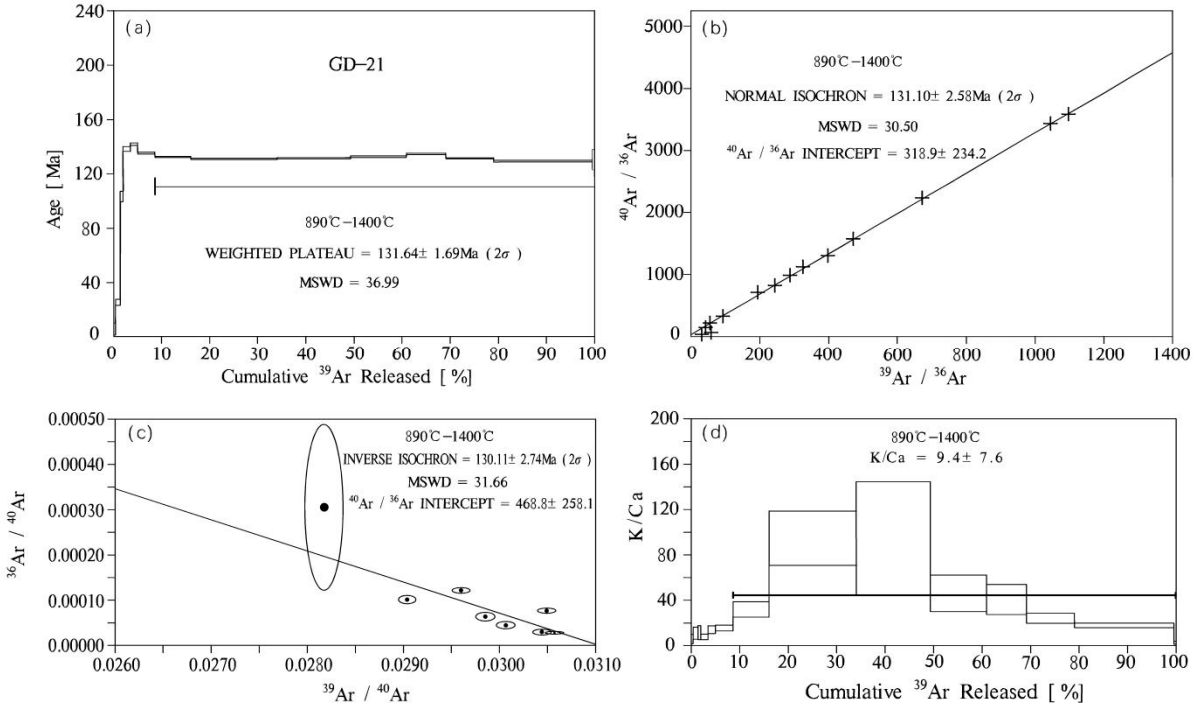


Figure 8. $^{40}Ar/^{39}Ar$ spectrum (**a**), isochronal age diagram (**b**), inverse isochronal age diagram (**c**), and K-Ca plateau (**d**) of phlogopite from the Guodian skarn Fe deposit.

The young apparent ages at the beginning of the step-heating experiment show that the outer part of the phlogopite grain experienced a severe thermal disturbance above its closure temperature. The ages from 890 °C to 1400 °C heating steps are between 129.45 ± 0.45 Ma and 134.73 ± 0.54 Ma, which shows that the inner part of the grain did not experience a severe thermal disturbance above its closure temperature. However, we think that the ages of the steps selected by us are not very scattered, and we can give an approximate age limit on the time of the event. We think the time of the Fe mineralization in Guodian is approximately 131.64 ± 1.69 Ma, and it might not be younger than 129.45 ± 0.45 Ma or older than 134.73 ± 0.54 Ma. Although the value of MSWD is a bit high, the plateau age is still meaningful to define the mineralization age in the region.

6. Discussion

6.1. Metallogenic Geological Characteristics

The skarn-type iron deposits in the Qihe–Yucheng region are mainly distributed in the contact zone between the Late Mesozoic intermediate–basic intrusive rocks and the Ordovician Majiagou group carbonate rocks or Carboniferous Permian clastic rocks. The iron ore bodies are obviously controlled by strata and rock mass, and their shapes, occurrences, and sizes are closely related to the occurrence of the strata–rock mass contact zone at the concave, convex, or inclined turning end, of which large-scale ore bodies are easily formed. The spatial occurrence forms of ore bodies are diverse, mainly including contact zone occurrence, fracture filling, interlayer filling, fracture penetration, xenolith structure, and other ore hosting forms [24], wherein the contact zone occurring state is the most important iron ore-bearing form in the area. The occurrence of deposits in the area is obviously controlled by regional faults. The inclined ends of the two wings of anticline in fold structure, the intersection of structures, and the interlayer fracture zone formed by tectonic action are all favorable metallogenic sites for iron ore in the area. The skarn high-grade iron ore deposits in the Qihe–Yucheng region have similar metallogenic geological characteristics as those in the Zibo and Laiwu areas, and they are controlled by a combination of magma, strata, and structure (Table 2). In addition, skarn assemblages in the Guodian iron deposit are composed chiefly of magnesium-rich skarn

minerals, e.g., forsterite, diopside, phlogopite, and serpentine, indicating that the carbonate wall rocks dominated by dolomite and dolomitic limestone underwent strong contact metasomatism during the formation of the Guodian iron deposit. As the magnesium skarn minerals do not contain iron, or the content of iron is very low, their formation cannot consume a large amount of iron in the ore-forming fluid [1], which can, in turn, facilitate the enrichment of iron in the fluid and eventually precipitation in the form of magnetite, promoting the formation of large-scale high-grade iron ore. Skarn assemblages in the Laiwu Zhangjiawa iron ore, the largest skarn high-grade iron deposit in the Luxi Block, are also dominated by magnesium skarn minerals [39]. This coincidence re-emphasizes the critical role of Mg-rich carbonate in skarn Fe mineralization [40].

Table 2. Geological characteristics of skarn iron ore in the Luxi Block

Mine	Typical Deposit	Ore-Forming Intrusions		Ore-Controlling Strata	Ore-Controlling Structure	Orebody Space Occurrence	Wall Rock Alteration and Metamorphism
		Intrusions	Lithology				
Qihe–Yucheng	Guodian	Pandian intrusion	Pyroxene diorite, diorite,	Ordovician dolomitic limestone, dolomite, Carboniferous–Permian sandstone and mudstone	The intersection of fault structures or the intersection of fault structures and the core of brachy anticline	Contact zone occurrence, interlayer filling, xenolith structure, fracture penetration	Skarnization, phlogopitization, serpentinization, sodium alteration, marblezation, keratinization
	Litun	Litun intrusion	Pyroxene diorite, hornblende diorite, quartz diorite	Carboniferous–Permian Sand–mudstone			
	Dazhang	Dazhang intrusion	Dioritic	Ordovician dolomitic limestone and limestone			
Zibo	Wang Wangzhuang	Jinling complex	Monzodiorite, hornblende diorite	Ordovician limestone and dolomitic limestone	Jinling brachy anticline	Contact zone occurrence	Potassic, sodium alteration, marbleza-tion,skarnization
Laiwu	Zhang Jiawa	Kuangshan pluton	Pyroxene diorite, diorite, monzonite, monzodiorite	Ordovician dolomite and dolomitic limestone	Mine anticline and its secondary folds	Contact zone occurrence, interlayer filling, xenolith structure, fracture penetration	Skarnization, phlogopitization, serpentinization, chloritization

6.2. Age of the Guodian Fe Deposit

The $^{40}Ar/^{39}Ar$ dating of potassium-bearing gangue minerals closely associated with ore minerals is an effective means to determine the metallogenic age of deposits, and it has been extensively used in the study of the metallogenic chronology of various hydrothermal deposits [41–43]. Phlogopite is a ubiquitous potassium-bearing mineral in skarn iron deposits and, particularly, it precipitates simultaneously with magnetite. The $^{40}Ar/^{39}Ar$ dating of phlogopite can thus place a tight constraint on the metallogenic age of skarn iron deposits [44,45]. In this study, phlogopite closely associated with magnetite was selected from a Guodian iron-rich ore body, which is an ideal object for accurately constraining the time of the iron-rich ore. The Ar-Ar isotopic system of phlogopite is very sensitive to late geological processes and is prone to being superimposed by late geological processes, resulting in an obvious diffusion loss spectrum [36,46], while the undisturbed phlogopite forms a flat age spectrum [37,45]. The apparent age of phlogopite measured is relatively stable in the medium- and high-temperature zones heated at the stage, and the age differences among different temperature zones are very small, forming a flat age spectrum without an abnormal age spectrum, indicating that the internal Ar isotopic composition remains stable upon formation of phlogopite and that no thermal disturbance higher than its closure temperature has occurred. Meanwhile, the test results of isochron age, inverse

isochron age, and plateau age show a high degree of agreement, which indicates that the test data are reliable. Thus the plateau age obtained (131.6 ± 1.7 Ma (MSWD = 36.99)) can represent the crystallization age of phlogopite.

Zhang Zhaonian [47] carried out microscopic temperature measurements of diopside and epidote fluid inclusions in iron deposits in the Qihe–Yucheng ore district. The temperature measurement results show that the homogenization temperature of fluid inclusions at the oxide stage (the main metallogenic stage) is between 390 °C and 410 °C. In addition, Zhao Yiming [48] performed a comprehensive analysis of the fluid characteristics and formation physicochemical conditions of the main skarn deposits in China. Through the statistics on homogenization temperature and burst temperature of 17 skarn deposits, it was concluded that the decrepitation temperature of magnetite in each deposit ranged from 540 to 300 °C (largely 380 to 480 °C). The $^{40}Ar/^{39}Ar$ closure temperature of phlogopite is approximately in the range of 400–480 °C [49,50]. The $^{40}Ar/^{39}Ar$ plateau age represents the age when the mineral cools to the closure temperature of the Ar isotopic system based on the principle of isotopic dating [51], all of which indicate that the cooling age of phlogopite obtained in this paper is approximately equal to the crystallization age of phlogopite. As mentioned above, phlogopite is closely associated with magnetite in the main ore stage. Therefore, the $^{40}Ar/^{39}Ar$ age of phlogopite approximately represents the formation age of phlogopite and magnetite. The $^{40}Ar/^{39}Ar$ plateau age of phlogopite reveals the Guodian iron mineralization formed at 131.6 ± 1.7 Ma. The zircon U-Pb age of the Pandian intrusion, which is spatially related to the Guodian deposit, is 124.4 ± 1.4 Ma [8]. Considering the accuracy of zircon U-Pb dating is about 4%, and even less than 10% in some cases [51,52], the zircon U-Pb age of the Pandian intrusion overlaps the $^{40}Ar/^{39}Ar$ age of phlogopite from the Guodian deposit. These results indicate that Guodian Fe mineralization is temporally and likely genetically related to Pandian diorite, which has promoted the formation of the skarn Fe deposit in the Guodian area.

6.3. A Causal Link between Iron Skarn Mineralization and Craton Destruction

The skarn iron deposits in NCC are mainly distributed in the depression zone at the edge of the NCC uplift or the edge of the secondary depression zone in the uplift. The Luxi Block is one of the crucial skarn-type high-grade iron ore metallogenic areas in the eastern NCC, which accounts for an important source of high-grade iron ore in China. Skarn iron deposits in the Luxi Block are primarily distributed in the Laiwu, Zibo, Jinan, and Qihe–Yucheng districts. The iron deposits in the Luxi Block are first-order structurally controlled by NNE trending deep faults and secondary faults of the NCC. Those skarn iron deposits are localized by the intersection of the nearly east–west trending fold structures, depression zones, or fault tectonic zones and the NNE or NE, NW trending structures [5]; they are genetically related to Mesozoic intermediate–basic intrusions (gabbro diorite, diorite, granodiorite, and monzonite) [2,53]. U-Pb dating of magmatic zircon and hydrothermal titanite and $^{40}Ar/^{39}Ar$ geochronology of phlogopite in the Laiwu Zhangjiawa iron deposit in the central part of the Luxi Block indicate that the timing of the Fe mineralization and associated mineralized intrusions in the Laiwu district are 133–130 Ma [4,5,54,55]. The Jinan and Zibo skarn iron ore deposits in the northern part of the Luxi Block are mainly related to the Jinan complex and the Zibo complex, respectively. The zircon U-Pb dating of ore-related complexes and the garnet U-Pb dating of the iron deposits show that the diagenetic and metallogenic ages are 130–128 Ma [5,56,57] (DuanZhuang, unpublished data). The skarn iron deposits in the Qihe–Yucheng ore district in the northwestern part of the Luxi Block are spatially related to the Litun, Dazhang, and Guodian intrusions, whose zircon U-Pb ages are 132–124 Ma [8,26] (Table 3, Figure 9). The present results, combined with existing isotopic age data, demonstrate that the skarn Fe mineralization and associated productive diorites in the Qihe–Yucheng ore district coincide with the iron mineralization and ore-forming intrusions in the Laiwu, Zibo, and Jinan areas, implying genetic links among them.

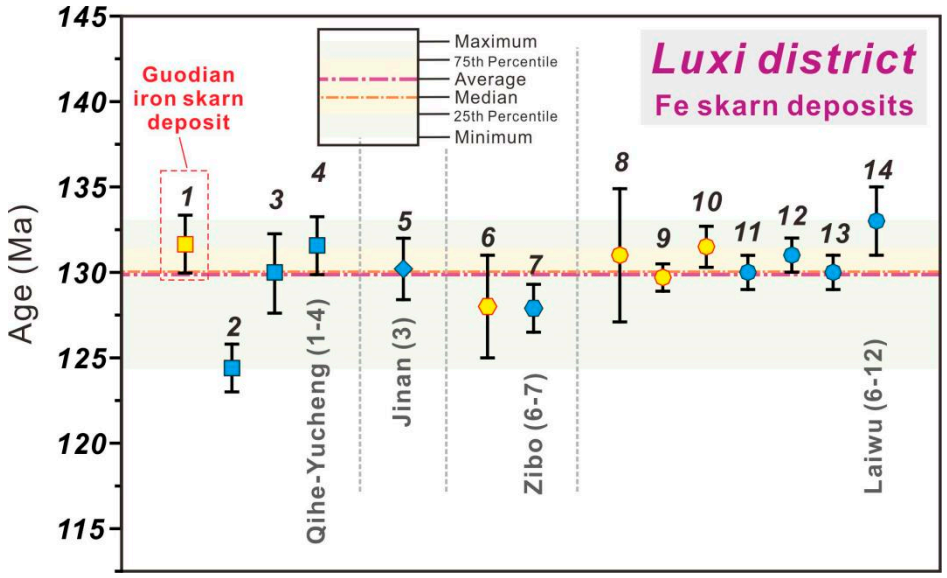


Figure 9. Age distribution of iron skarn mineralization and ore-related magmatism in the Luxi district. (The yellow and blue graphics with different shapes represent the age data of mineralization and related intrusions, respectively. The numbers represent the age data numbers in Table 3 and the number annotations in Figure 1).

Table 3. Age date of the Mesozoic skarn Fe deposits and related intrusions in the North China Craton.

Mining Area	Intrusion/Deposit	Number	Sample	Analytical Method	Age (Ma)	References
Qihe-yucheng	Guodian iron deposit	1	Phlogopite-bearing iron ores	Phlogopite ^{40}Ar-^{39}Ar Dating	131.64 ± 1.69	This study
	Guodian intrusions	2	Diorite	Zircon U-Pb dating	124.4 ± 1.4	[8]
	Litun intrusions	3	Diorite	Zircon U-Pb dating	130 ± 2.3	[26]
	Dazhang intrusions	4	Diorite	Zircon U-Pb dating	131.6 ± 1.7	
Ji'nan	Zhangmatun intrusions	5	Gabbro	Zircon U-Pb dating	130.2 ± 1.8	[57]
Zibo	Zhaokou iron deposit	6	Garnet skarn	Garnet U-Pb dating	128 ± 3	[5]
	Jinling intrusions	7	Biotite diorite	Zircon U-Pb dating	127.9 ± 1.4	[56]
Laiwu	Zhangjiawa iron deposit (I)	8	Skarn	Sphene U-Pb dating	131 ± 3.9	[4]
		9	Phlogopite-bearing iron ores	Phlogopite ^{40}Ar-^{39}Ar Dating	129.7 ± 0.8	[5]
	Zhangjiawa iron deposit (Gangli)	10	Phlogopite-bearing iron ores	Phlogopite ^{40}Ar-^{39}Ar Dating	131.5 ± 1.2	
	Kuangshan intrusions	11	Diorite	Zircon U-Pb dating	130 ± 1	[4]
	Jiaoyu intrusions	12	Diorite	Zircon U-Pb dating	131 ± 1	[55]
	Jinniushan intrusions	13	Diorite	Zircon U-Pb dating	130 ± 1	
	Tietonggou intrusions	14	Pyroxene diorite	Zircon U-Pb dating	133 ± 2	[56]

Unlike most other cratons across the planet, the lithosphere thickness of the NCC in the Paleozoic and Cenozoic is hugely different, and the lithosphere of the NCC has been significantly activated and transformed [58–61]. From the perspective of regional tectonic evolution, the NCC, especially its eastern part, has experienced strong crustal extension, lithospheric thinning, and cratonic destruction since the Mesozoic, and large-scale tectonic deformation and magmatic activities have taken place [18,62–65]. The destruction of the integrity of the eastern part of the North China Craton is closely related to the heterogeneous

flow of the mantle caused by the subduction of the Pacific plate [18]. The destruction of the eastern part of the North China Craton culminated in the Early Cretaceous (~125 Ma).

Based on a comprehensive analysis of the geological and structural features in Shandong province, some studies conclude that the geodynamic evolution of metallogenesis is mainly controlled by the collisional orogeny of the Yangtze and the North China plates as well as subduction of the Paleopacific plate. It has been further divided into six periods of continental collisional orogen in the Late Triassic, the transformation from passive to active continental margin and crustal accretion in the Middle Jurassic, the transformation from crust accretion to collapse in the Early Cretaceous, the large-scale delamination of lithosphere and intense crust–mantle interaction in the Early Cretaceous, the subduction of the continental margirarc, and the intense extension of the postare lithosphere in the Late Cretaceous, corresponding to the following six phases of gold and polymetallic metallogenesis: ~205 Ma, 160~155 Ma, 135~125 Ma, 125~115 Ma, 115~100 Ma, and 100~90 Ma, respectively [66]. In the Luxi district, the timing of iron skarn mineralization is concentrated at ~130 Ma, which corresponds to the tectonic setting of the transformation from crust accretion to collapse in the Early Cretaceous (135~125 Ma).

As mentioned above, the skarn iron mineralization (~130 Ma) in the Luxi Block was concurrent or quasi-concurrent with the culmination of the destruction of the NCC, implying the extensive skarn iron mineralization might be the responses and products of the lithosphere destruction of the NCC. In addition to the Luxi Block, iron mineralization of similar ages is also well developed in several major iron-producing regions on the eastern NCC, e.g., Handan–Xingtai district, Xuhuai district, and Linfen district, suggesting that iron deposits in these districts formed under the same geodynamic setting, i.e., the destruction of NCC. The removal of the lithosphere, coupled with the upwelling of the hot asthenosphere, generated voluminous basic–intermediate magmas that could have provided heat energy, fluids, chlorine, and Fe, contributing to the large-scale Fe mineralization in the NCC. Additional chlorine and Fe may have originated from Ordovician carbonate rocks [67]. Crustal fracture systems associated with the lithospheric extension served as ideal sites for fluid circulation and iron mineralization.

7. Conclusions

The Guodian iron deposit and the other high-grade skarn Fe deposits in the Luxi district have similar metallogenic geological characteristics and share the general characteristics of "strata, magmatic rock, and structure" joint control. The $^{40}Ar/^{39}Ar$ isotopic age of phlogopite associated with magnetite within iron ore samples from the Guodian skarn iron deposit is 131.6 ± 1.7 Ma. Based on published geochronological data of skarn deposits and metallogenic rocks in the Luxi Block, the large-scale skarn iron mineralization and associated ore-forming magmas in the Luxi Block formed in the Early Cretaceous (~130 Ma), which is consistent with the peak period of North China Craton destruction, indicating that the large-scale skarn iron mineralizations in the Luxi Block, including that of the Qihe–Yucheng region, are the responses and products of lithospheric thinning and destruction of the North China Craton. Lithospheric thinning and destruction have significantly facilitated pervasive Fe mineralization by providing sufficient heat energy, fluids, chlorine, and Fe, in addition to favorable structural sites for fluid flow and Fe deposition.

Author Contributions: Conceptualization, Q.F.; sampling and experiments, Q.F., S.L., B.W., M.M., C.F. and Z.D. (Zhicai Dang); data analysis and figures, S.L., C.F., Y.L., Z.W. and Y.Z.; writing—original draft preparation, M.G.; writing—review and editing, Q.F., S.L., Z.D. (Zhuang Duan) and J.G. All authors have read and agreed to the published version of the manuscript.

Funding: This research was supported by the Provincial geological exploration projects of Shandong Province (SDGP370000202002001782), Technology research projects of Shandong Provincial Bureau of Geology and Mineral Resources, and the Open Fund of No. 1 Institute of Geology and Mineral Resources of Shandong Province (2021DW03, 2022DW01).

Data Availability Statement: The data used to support the findings of this study are included within this article.

Acknowledgments: We are grateful to the academic editor and anonymous reviewers, whose constructive suggestions greatly improved our manuscript.

Conflicts of Interest: The authors declare no conflicts of interest.

References

1. Zhang, Z.C.; Li, H.M.; Li, J.W.; Song, X.Y.; Hu, H.; Li, L.F.; Chai, F.M.; Hou, T.; Xu, D.R. Geological settings and metallogenesis of high-grade iron deposits in China. *Sci. China Earth Sci.* **2021**, *64*, 691–715. [CrossRef]
2. Zhang, Z.C.; Hou, T.; Li, H.M.; Li, J.W.; Zhang, Z.H.; Song, X.Y. Enrichment mechanism of iron in magmatichydrothermal system. *Acta Petrol. Sin.* **2014**, *30*, 1189–1204.
3. Deng, X.D.; Li, J.W.; Wen, G. U-Pb Geochronology of Hydrothermal Zircons from the Early Cretaceous Iron Skarn Deposits in the Handan-Xingtai District, North China Craton. *Econ. Geol.* **2015**, *110*, 2159–2180. [CrossRef]
4. Duan, Z.; Li, J.W. Zircon and titanite U-Pb dating of the Zhangjiawa iron skarn deposit, Luxi district, North China Craton:implications for a craton-wide iron skarn mineralization. *Ore Geol. Rev.* **2017**, *89*, 309–323. [CrossRef]
5. Duan, Z.; Gao, M.B.; Gao, J.L.; Li, C.J.; Feng, Q.W.; Li, S.Y.; Gao, W.S.; Wang, X.Z.; Xu, Z.Y.; Li, J.W. Phlogopite $^{40}Ar/^{39}Ar$ dating of the Zhangjiawa iron deposit, Laiwu district, Shandong Province: Implications for regional iron skarn mineralization of North China Craton. *Acta Geol. Sin.* **2022**, *96*, 1279–1296. [CrossRef]
6. Zheng, J.M.; Xie, G.Q.; Liu, J.; Chen, M.H.; Wang, S.M.; Guo, S.F.; Gao, X.; Li, G.D. $^{40}Ar/3^{9}Ar$ dating of phlogopite from the Xishimen skarn deposit in the Handan Xingtai area, southern Hebei, and its implications. *Acta Petrol. Sin.* **2007**, *23*, 2513–2518. [CrossRef]
7. Shen, J.; Li, S.; Santosh, M.; Dong, G.; Wang, Y.; Liu, H.; Peng, Z.; Zhang, Z. Zircon U-Pb geochronology of the basement rocks and dioritic intrusion associated with the Fushan skarn iron deposit, southern Taihang Mountains, China. *J. Asian Earth Sci.* **2015**, *113*, 1132–1142. [CrossRef]
8. Qin, J.; Zhu, X.Q.; Wang, L.J.; Hao, X.Z. Ore-forming Origin of Rock Mass Zircon U-Pb Chronology and Geochemical Evidence of Pandian Iron Deposit in Luxi Area. *Shandong Land. Resour.* **2023**, *39*, 14–22. [CrossRef]
9. Griffin, W.L.; Zhang, A.D.; O'reilly, S.Y.; Ryan, C.G. Phanerozoic evolution of the lithosphere beneath the Sino-Korean craton. In *Mantle Dynamics and Plate Interactions in East Asia*, 1st ed.; Flower, M.F.J., Chung, S.L., Lo, C.H., Lee, T.Y., Eds.; American Geophysical Union: Washington, DA, USA, 1998; Volume 27, pp. 107–126.
10. Fan, W.M.; Zhang, H.F.; Baker, J.; Jarvis, K.E.; Mason, P.R.D.; Menzies, M.A. On and off the North China Craton: Where is the Archaean keel? *J. Petrol.* **2000**, *41*, 933–950. [CrossRef]
11. Gao, S.; Rudnick, R.L.; Yuan, H.L.; Liu, X.M.; Liu, Y.S.; Xu, W.L.; Ling, W.L.; Ayers, J.; Wang, X.C.; Wang, Q.H. Recycling lower continental crust in the North China craton. *Nature* **2004**, *432*, 892–897. [CrossRef]
12. Kusky, T.M.; Windley, B.F.; Zhai, M.G. Tectonic evolution of the North China Block:from orogen to craton to orogen. *Geol. Soc.* **2007**, *280*, 1–34. [CrossRef]
13. Menzies, M.; Xu, Y.G.; Zhang, H.F.; Fan, W.M. Integration of geology, geophysics and geochemistry: A key to understanding the North China Craton. *Lithos* **2007**, *96*, 1–21. [CrossRef]
14. Gao, S.; Zhang, J.F.; Xu, W.L.; Liu, Y.S. Delamination and destruction of the North China Craton. *Chin. Sci. Bull.* **2009**, *54*, 3367. [CrossRef]
15. Wilde, S.A.; Zhou, X.; Nemchin, A.A.; Sun, M. Mesozoic crust-mantle interaction beneath the North China craton: A consequence of the dispersal of Gondwanaland and accretion of Asia. *Geology* **2003**, *31*, 817–820. [CrossRef]
16. Wu, F.Y.; Walker, R.J.; Yang, Y.H.; Yuan, H.L.; Yang, J.H. The chemical-temporal evolution of lithospheric mantle underlying the North China Craton. *Geochim. Et Cosmochim. Acta* **2006**, *70*, 5013–5034. [CrossRef]
17. Zhai, M.G.; Bian, A.G.; Zhao, T.P. The amalgamation of the supercontinent of North China Craton at the end of Neo-Archaean and its breakup during late Palaeoproterozoic and Meso-Proterozoic Science in China series D. *Earth Sci.* **2000**, *43*, 219–232. (In Chinese) [CrossRef]
18. Zhu, R.X.; Chen, L.; Wu, F.Y.; Liu, J.L. Timing, scale and mechanism of the destruction of the North China Craton. *Sci. China Earth Sci.* **2011**, *54*, 789–797. [CrossRef]
19. Xu, W.L.; Wang, D.Y.; Wang, Q.H.; Pei, F.P.; Lin, J.Q. $^{40}Ar/^{39}Ar$ dating of hornblende and biotite in Mesozoic intrusive complex from the North China Block: Constraints on the time of lithospheric thinning. *Geochimica* **2004**, *33*, 221–231. [CrossRef]
20. Yang, C.H.; Xu, W.L.; Yang, D.B.; Liu, C.C.; Liu, X.M.; Hu, Z.C. Petrogenesis of the Mesozoic High-Mg Diorites in West Shandong: Evidence from Chronology and Petro-geochemistry. *Earth Sci.-J. China Univ. Geosci.* **2006**, *31*, 81–92.
21. Zhu, R.X.; Xu, Y.G.; Zhu, G.; Zhang, H.F.; Xia, Q.K.; Zheng, T.Y. Destruction of the North China Craton. *Sci. China Earth Sci.* **2012**, *55*, 1565–1587. [CrossRef]
22. Duan, Z. The Mineralization and Mechanism of the Iron Skarn Deposits in Laiwu District, Shandong Province. Doctoral Thesis, China University of Geosciences (Wuhan), Wuhan, China, 2019.
23. Hao, X.Z.; Zheng, J.M.; Liu, W.; Wang, R.S.; Wang, Q.Y.; Zhang, G.L. Metallogenic Prognosis of Skarn-type Iron Ore Deposits in Qihe–Yucheng Area, Shandong Province. *Acta Geosci. Sin.* **2020**, *41*, 293–302. [CrossRef]

24. Hao, X.Z.; Zhang, G.L.; Liu, W.; Wang, R.S.; Li, Y.P.; Zhi, Y.B.; Wang, J.G. Prospecting methods of skarn type iron deposit in Dezhou area, Shandong Province. *Miner. Explor.* **2020**, *11*, 1219–1227.
25. Wang, R.S.; Hao, X.Z.; Chen, D.L.; Chen, H.J.; Liu, H.B.; Wang, H.J.; Yu, L.; Li, R.; Liu, H.; Liu, W. Discussion on the boundary of metallogenic geological body of skarn type iron deposits and study on its deep characteristics in Qihe-Yucheng area, Sshandong Province. *Prog. Geophys.* **2022**, *37*, 59–68. [CrossRef]
26. Hao, X.Z.; Guo, Y.M.; Li, Y.P.; Wang, J.G.; Zhang, C.C.; Wang, Q.Y.; Liu, B.B.; Zhi, Y.B. Metallogeny of the skarn-type iron deposits in Qihe-Yucheng ore district, Shandong Province. *J. Geol.* **2019**, *43*, 566–572. [CrossRef]
27. Liu, S.; Hu, R.Z.; Gao, S.; Feng, C.X.; Qi, L.; Zhong, Z.; Xiao, T.; Qi, Y.Q.; Wang, T.; Coulson, I.M. Zircon U-Pb geochronology and major, traceelemental and Sr-Nd-Pb isotopic geochemistry of mafic dykes inwestern Shandong Province, East China: Constrains on their petro-genesis and geodynamic significance. *Chem. Geol.* **2008**, *255*, 329–345. [CrossRef]
28. Wang, S.S. Age determinations of ^{40}Ar-^{40}K, ^{40}Ar-^{39}Ar and radiogenic ^{40}Ar released characteristics on K-Ar geostandards. *Chin. J. Geol.* **1983**, *4*, 315–323.
29. Steiger, R.H.; Jager, E. Subcommission on geochronology: Convention on the use of decay constants in geo-and cosmochronology. *Earth Planet. Sci. Lett.* **1977**, *36*, 359–362. [CrossRef]
30. Nier, A.O. A redetermination of the relative abundances of the isotope of carbon, nitrogen, oxygen, argon, and potassium. *Phys. Rev.* **1950**, *77*, 789–793. [CrossRef]
31. Koppers, A.A.P. ArArCALC-software for ^{40}Ar/^{39}Ar age calculations. *Comput. Geosci.* **2002**, *28*, 605–619. [CrossRef]
32. Dalrymple, G.B.; Lanphere, M.A. *Potassium-Argon Dating*; W. H. Freeman Co.: San Fransisco, CA, USA, 1969.
33. Fleck, R.J.; Sutter, J.F.; Elliot, D.H. Interpretation of discordant ^{40}Ar/^{39}Ar age-spectra of Mesozoictholeiites From Antarctica. *Geochim. Cosmochim. Acta* **1977**, *41*, 15–32. [CrossRef]
34. Lanphere, M.A.; Dalrymple, G.B. The use of ^{40}Ar/^{39}Ar data in evaluation of disturbed K-Ar systems. *U. S. Geol. Surv. Open-File Rep.* **1978**, *701*, 241–243.
35. Pringle, M.S. Age progressive volcanism in the Musicians Seamounts: A test of the hot spot hypothesis for the late Cretaceous Pacific. In *The Mesozoic Pacific: Geology, Tectonics, and Volcanism*; Pringle, M.S., Sager, W.W., Sliter, W.V., Stein, S., Eds.; American Geophysical Union: Washington, DC, USA, 1993; pp. 187–216.
36. Hanson, G.N.; Smimons, K.P.; Bence, A.E. ^{40}Ar/^{39}Ar spectrumages for biotite, hornblende and muscovite in a contact metamorphic zone. *Geochim. Et Cosmochim. Acta* **1975**, *39*, 1269–1278. [CrossRef]
37. Qiu, H.N.; Bai, X.J. Fluid Inclusion ^{40}Ar/^{39}Ar Dating Technique and Its Applications. *Earth Sci.* **2019**, *44*, 685–697. [CrossRef]
38. Yuan, S.D.; Liu, X.F.; Wang, X.D.; Wu, S.H.; Yuan, Y.B.; Li, X.K.; Wang, T.Z. Geological characteristics and ^{40}Ar-^{39}Argeochronology of the Hongqiling tin deposit in southern Hunan Province. *Acta Petrol. Sin.* **2012**, *28*, 3787–3797.
39. Peng, J.T.; Zhou, M.F.; Hu, R.Z.; Shen, N.P.; Yuan, S.D.; Bi, X.W.; Du, A.D.; Qu, W.J. Precise molybdenite Re-Os and mica Ar-Ar dating of the Mesozoic Yaogangxian tungsten deposit, Central Nanlingdistrict, South China. *Miner. Depos.* **2006**, *41*, 661–669. [CrossRef]
40. Meinert, L.D.; Dipple, G.M.; Nicolescu, S. *World Skarn Deposits: ECONOMIC Geology 100th Anniversary Volume*; Society of Economic Geologists: Littleton, CO, USA, 2005; pp. 299–336. [CrossRef]
41. Peng, J.T.; Hu, R.Z.; Bi, X.W.; Dai, T.M.; Li, Z.L.; Li, X.M.; Shuang, Y.; Yuan, S.D.; Liu, S.R. ^{40}Ar/^{39}Ar isotopic dating of tin mineralization in Furong deposit of Hunan Province and its geological significance. *Miner. Depos.* **2007**, *26*, 237–248. (In Chinese)
42. Yuan, S.D.; Peng, J.T.; Shen, N.P.; Hu, R.Z.; Dai, T.M. ^{40}Ar-^{39}Ar isotopic dating of the Xianghualing Sn-polymetallic orefield in southern Hunan, China and its geological implications. *Acta Geol. Sinica* **2015**, *81*, 278–286. [CrossRef]
43. Xie, G.q.; Mao, J.W.; Zhao, H.J.; Duan, C.; Yao, L. Zircon U-Pb Aad phlogopite ^{40}Ar/^{39}Ar Age of the Chengchao and jinshandian skarn Fedposits, southeast Hubei Province, Middle Lower Yangtze River Vallet metallogenicbelt, China. *Miner. Depos.* **2012**, *47*, 633–652. [CrossRef]
44. Li, J.W.; Vasconcelos, P.M.; Zhou, M.F.; Deng, X.D.; Cohen, B.; Bi, S.J.; Zhao, X.F.; Selby, D. Longevity of magmatic-hydrothermal systems in the Daye Cu-Fe-Au sistrict, eastern China with implications for mineral exploration. *Ore Geol. Rev.* **2014**, *57*, 375–392. [CrossRef]
45. Chen, W.; Wan, Y.S.; Li, H.Q.; Zhang, Z.Q.; Dai, T.M.; Shi, Z.E.; Sun, J.B. Isotope Geochronology: Technique and Application. *Acta Geol. Sin.* **2011**, *85*, 1917–1947.
46. Snee, L.W.; Sutter, J.F.; Kelly, W.C. Thermochronology of economic mineral deposits; dating the stages of mineralization at panasqueira, portugal, by high-precision 40/39 Ar age spectrum techniques on muscovite. *Econ. Geol.* **1988**, *83*, 335–354. [CrossRef]
47. Zhang, Z.N.; Cao, Y.; Zhu, Y.Z.; Pang, Z.S.; Shen, L.J.; Guan, J.Y.; Guo, C.F. Enrichment mechanism of iron in Dazhang skarn iron deposit, Shandong Province: Evidence from fluid inclusions and hydrogen-oxygen isotopes. *Miner. Depos.* **2022**, *41*, 91–105. [CrossRef]
48. Zhao, Y.M.; Lin, W.W.; Bi, C.S.; Li, D.X. Basic Geological Characteristics of skarn deposits of China. *Bull. Chin. Acad. Geol. Sci.* **1986**, *8*, 59–87.
49. Dodson, M.H. Closure temperature in cooling geochronological andpetrological systems. *Contrib. Mineral. Petrol.* **1973**, *40*, 259–274. [CrossRef]
50. Giletti, B.J.; Tullis, J. Studies in diffusion: Pressure dependence of Ar diffusion in phlogopite mica. *Earth Planet. Sci. Lett.* **1977**, *35*, 180–183. [CrossRef]

51. Klötzli, U.; Klötzli, E.; Günes, Z.; Kosler, J. *Accuracy of Laser Ablation U-Pb Zircon Dating: Results from a Test Using Five Different Reference Zircons*; Blackwell Publishing Ltd.: Hoboken, NJ, USA, 2009. [CrossRef]
52. Li, X.H.; Liu, X.M.; Liu, Y.S.; Su, L.; Sun, W.D.; Huang, H.Q.; Yi, K. Accuracy of LA-ICPMS zircon U-Pb age determination: An inter-laboratory comparison. *Sci. China Earth Sci.* **2015**, *58*, 1722–1730. [CrossRef]
53. Zhang, B.T.; Hu, Z.G.; Cao, C.C.; Jiang, X.P.; Mei, Z.H.; Li, Z.P.; Du, L.M.; Hua, B.; Zhao, L.; Liu, S. Iron richpreexploration potential and favorable sites for deep horizon of Jinling maticcomplexdistribution in Zibo, Shandong Province. *Acta Geol. Sin.* **2021**, *95*, 1545–1560.
54. Yang, Q.L.; Zhao, Z.F.; Zheng, Y.F. Slab mantle interaction in continental subduction channel: Geochemical evidence from Mesozoic gabbroic intrusives in southeastern North China. *Lithos* **2012**, *155*, 442–460. [CrossRef]
55. Lan, T.G.; Hu, R.Z.; Chen, Y.H.; Wang, H.; Tang, Y.W.; Liu, L. Generation of high Mgdiorites and associated iron mineralization within an intracontinental setting: Insights from ore-barren and oer-bearing intrusions in the eastern North China Craton. *Gondwana Res.* **2019**, *72*, 97–119. [CrossRef]
56. Jin, Z.L.; Zhang, Z.C.; Hou, T.; Santosh, M.; Han, L. Geneticrelationship of high-Mg diorotic pluton to iron mineralization: A case study from the Jinling skarn type iron deposit in the North China Craton. *J. Asian Earth Sci.* **2015**, *113*, 957–979. [CrossRef]
57. Xie, Q.H.; Zhang, Z.C.; Hou, T.; Santosh, M.; Jin, Z.L.; Han, L.; Cheng, Z.G. Petrogenesis of the Zhangmatun gabbro in the Ji'nan Comples, North China Craton: Implications for skarn-type iron mineralization. *J. Asian Earth Sci.* **2015**, *113*, 1197–1217. [CrossRef]
58. Fan, W.M.; Menzies, M.A. Destruction of aged lower lithosphere and accretion of asthenosphere mantle beneath eastern China. *Geotecton. Et Metallog.* **1992**, *16*, 171–180.
59. Menzies, M.A.; Fan, W.M.; Zhang, M. Palaeozoic and Cenozoic lithoprobes and the loss of >120 km of Archaean lithosphere, Sino-Korean craton, China. *Geol. Soc.* **1993**, *76*, 71–81. [CrossRef]
60. Deng, J.F.; Mo, X.X.; Zhang, H.L.; Luo, Z.H.; Du, Y.S. Lithosphere root/de-rooting and activation of the east China continent. *Geoscience* **1994**, *8*, 349–356.
61. Menzies, M.A.; Xu, Y.G. Geodynamics of the North China Craton. In *Mantle Dynamics and Plate Interactions in East Asiain*, 1st ed.; Flower, M.F.J., Chung, S.L., Lo, C.H., Lee, T.Y., Eds.; American Geophysical Union: Washington, DA, USA, 1998; Volume 27, pp. 155–165.
62. Yang, J.H.; Wu, F.Y.; Wilde, S.A. A review of the geodynamic setting of large-scale Late Mesozoic gold mineralization in the North China Craton: An association with lithospheric thinning. *Ore Geol. Rev.* **2003**, *23*, 125–152. [CrossRef]
63. Wu, F.Y.; Lin, J.Q.; Wilde, S.A.; Zhang, X.; Yang, J.H. Nature and significance of the Early Cretaceous giant igneous event in eastern China. *Earth Planet. Sci. Lett.* **2005**, *233*, 103–119. [CrossRef]
64. Liu, J.L.; Ji, L.; Ni, J.L.; Chen, X.Y. Dynamics of the Early Cretaceous lithospheric thinning and destruction of the North China craton as the consequence of Paleo-Pacific type active continental margin. *Acta Geol. Sin.* **2022**, *96*, 3360–3380. [CrossRef]
65. Ma, M.; Zhang, C.; Li, Y.D.; Gao, M.B.; Gao, J.L.; Li, S.Y.; Feng, Q.W.; Li, J.; Cui, T.; Liu, Y.K. Geochronological, Geochemical and Sr-Nd-Pb-Hf isotopic constraints on the petrogenesis of pyroxene diorites in the Sanchahe iron-gold deposit, Western Shandong. *Minerals* **2022**, *12*, 601. [CrossRef]
66. Ding, Z.J.; Sun, F.Y.; Liu, F.L.; Liu, J.H.; Peng, Q.M.; Ji, P.; Li, B.L.; Zhang, P.J. Mesozoic geodynamic evolution and metallogenic series of major metal deposits in Jiaodong Peninsula, China. *Acta Petrol. Sin.* **2015**, *31*, 3045–3080.
67. Li, S.Y.; Duan, Z.; Gao, J.L.; Hu, H.; Wen, G.; Li, J.W. Controls on metal fertility of dioritic intrusions in the Laiwu district, North China craton: Insights from wholerock geochemistry and mineral compositions. *Geol. Soc. Am. Bull.* **2023**, *136*, 1287–1308. [CrossRef]

Disclaimer/Publisher's Note: The statements, opinions and data contained in all publications are solely those of the individual author(s) and contributor(s) and not of MDPI and/or the editor(s). MDPI and/or the editor(s) disclaim responsibility for any injury to people or property resulting from any ideas, methods, instructions or products referred to in the content.